Journal of Solid State Electrochemistry (2021) 25:1807–1813
https://doi.org/10.1007/s10008-021-04951-9

ORIGINAL PAPER

One-step CZT electroplating from alkaline solution on flexible Mo foil for CZTS absorber

C. Marchi[1] · G. Panzeri[1] · L. Pedrazzetti[1] · M. I. Khalil[1] · A. Lucotti[2] · J. Parravicini[3] · M. Acciarri[3] · S. Binetti[3] · L. Magagnin[1]

Received: 27 February 2021 / Revised: 6 April 2021 / Accepted: 12 April 2021 / Published online: 21 April 2021

Abstract

In this work, Cu-Zn-Sn (CZT) is co-electrodeposited onto a flexible Mo substrate exploiting an alkaline bath (pH 10). The plating solution is studied by cyclic voltammetry, highlighting the effects of potassium pyrophosphate ($K_4P_2O_7$) and EDTA-Na_2 on the electrochemical behavior and stability of the metallic ionic species. The optimized synthesis results in a homogeneous precursor layer, with composition Cu 44 ± 2 at. %, Zn 28 ± 1 at. %, and Sn 28 ± 2 at. %. Soft and reactive annealing are employed respectively to promote intermetallic phase formation and sulfurization of the precursor to obtain CZTS. Microstructural (XRD, Raman), morphological (SEM), and compositional (EDX, XRF) characterization is carried out on CZT and CZTS films, showing a minor presence of secondary phases. Finally, photo-assisted water splitting tests are performed considering a CZTS/CdS/Pt photoelectrode, showing a photocurrent density of 1.01 mA cm^{-2} at 0 V vs. RHE under 1 sun illumination.

Keywords Co-electrodeposition · Complexation · CZTS photoelectrode · Flexible molybdenum · Photo-water splitting

Introduction

Nowadays, the need for green and renewable energy sources is urgent and solar technologies are one of the leading fronts of the new era of energy production. In particular, photovoltaics had significant advancements in the last decades, showing a continuous improvement in the energy conversion efficiency achieved through new device architectures and employed materials (e.g., CdTe, CIGS, perovskite) [1]. The development of a thin-film technology aimed at lower production costs to maximize the diffusion of the photovoltaic market and enlarge the realm of possible applications, e.g., photo-assisted water splitting. In this view, one of the most investigated absorber materials is Cu_2ZnSnS_4 (CZTS): a p-type material characterized by a high absorption coefficient (>10^4 cm^{-1}) and a direct bandgap of ~1.5 eV [2]. Moreover, the employment of non-toxic, low-cost, and earth-abundant elements is the primary advantage of this material that, in combination with scalable fabrication techniques, possesses all the qualities to meet the requirements for affordable and sustainable photoactive films.

In this context, the traditional synthesis route comprises the deposition of the metallic precursors (Cu, Zn, Sn) followed by annealing in a sulfur atmosphere to promote the kesterite phase formation. Among all the available synthesis methods, electrodeposition has been considered a viable process, alternative to vacuum-based ones, because of its potential low cost and the capability to grow films over-large surface area [3]. Furthermore, the electrochemical deposition technique effectively controls the stoichiometry and ratios between the required crystalline phases, leading to highly photoactive chalcogenide films [4, 5]. Two main different electrochemical synthesis routes have been proposed in the literature: the stack elemental layer (SEL) approach [6], which comprises the sequential deposition of the copper, tin, and zinc layers (Cu/Sn/Zn), and the co-electrodeposition one, where all the elements are electrodeposited (Cu-Zn-Sn) from a single bath [7]. The former presents limitations in stacking order and requires multiple electrodeposition setups, but the stoichiometry of the metallic stack can be easily controlled [3].

✉ L. Magagnin
luca.magagnin@polimi.it

[1] Department of Chemistry, Materials and Chemical Engineering "Giulio Natta", Politecnico di Milano, Via Mancinelli 7, 20131 Milan, Italy

[2] Department of Chemistry, Materials and Chemical Engineering "Giulio Natta", Politecnico di Milano, Piazza Leonardo da Vinci 32, 20133 Milan, Italy

[3] Department of Materials Science and Solar Energy Research Centre (MIB-SOLAR), University of Milano - Bicocca, Via Cozzi 55, 20125 Milan, Italy

On the other hand, the latter requires a single experimental apparatus, but the challenge resides in formulating a stable deposition bath capable of growing a homogeneous film in thickness and composition over a large area [3]. Co-electrodeposition is traditionally carried out in acidic solution [8–10], where copper, tin, and zinc species are stable as divalent cations. Such an approach results in good bath stability. However, poor film morphology can be expected due to mass-limited transport and hydrogen evolution. Because of this reason, most of the studies focus on the role of complexing agents to further reduce the difference in reduction potential of the dissolved metallic species leading to improved photoactivity [11–15]. In this context, an alkaline medium can be a valid strategy to reduce the detrimental effects of hydrogen and the overall quality of the growing deposit.

In the present study, we report the co-electrodeposition of the CZT (Cu-Zn-Sn) metallic precursor layer from an alkaline solution on a flexible Mo-foil, followed by annealing/sulfurization treatment to obtain CZTS. Given the inherent disparity of the three metallic ions' reduction potentials [16, 17], the main focus is on the deposition bath's formulation. To demonstrate the synthesis method's viability, the photoactivity of the kesterite layer (CZTS/CdS/Pt) is evaluated through a photoelectrochemical water splitting test, showing photocurrents of ~1 mA cm^{-2} at 0 V vs. RHE in a sulfate solution buffered at pH = 6.85.

Experimental

The electrolytic solution was prepared by dissolving the appropriate amounts of potassium pyrophosphate ($K_4P_2O_7$), copper chloride ($CuCl_2{\cdot}2H_2O$), zinc sulfate ($ZnSO_4{\cdot}7H_2O$), EDTA-Na_2 and tin chloride ($SnCl_2{\cdot}2H_2O$) in 100 ml of Millipore water. The chemicals provided by Sigma-Aldrich and CARLO ERBA Reagents were used as received. The electrodeposition and the electrochemical tests were carried out at room temperature without agitation, using a molybdenum foil substrate of 0.2-mm thickness (GOODFELLOW) as a working electrode (WE). Before each deposition, Mo foil (1.5 × 1.5 cm^2) was cleaned by dipping in HCl 32%, followed by rinsing in water/acetone. A ruthenium-based mixed metal oxide (MMO) anode was used as a counter electrode (CE), and a saturated Ag/AgCl (3 M) (SSC) electrode (E_{SSC} = +0.210 V vs. RHE at 25 °C) was used as a reference electrode (RE). Inside the beaker, electrodes were arranged in a vertical configuration with the working electrode (WE) facing the CE, with the RE in between them, closer to the WE. The deposition was performed using AMEL 2553 Potentiostat/Galvanostat under galvanostatic conditions (−2.3 mA cm^{-2}, 10 min). The co-electrodeposition bath was developed through the optimization of the work of Khalil et al. [18–20] and comprised 230 mM of $K_4P_2O_7$, 15 mM of $CuCl_2$, 35 mM of $ZnSO_4$, 15 mM of EDTA-Na_2, 10 mM of $SnCl_2$, pH = 10 adjusted with NH_4OH. Soft (300 °C, 90 min) and reactive (560 °C, 20 min) annealing were carried out using a single-zone tubular furnace using N_2 as inert/carrier gas. For the reactive annealing, 20 mg of elemental sulfur and a flow of 5 L/h N_2 were used as standard setup. The X-ray fluorescence (XRF) analysis was performed using a FISCHERSCOPE X-RAY XAN. Each sample was measured on five spots to obtain a larger area reading of the average composition. X-ray diffraction (XRD) was carried out using a Phillips diffractometer PW 1830, and the crystalline phases were assigned based on Joint Committee on Powder Diffraction Standards (JCPDS). Scanning electron microscopy (SEM) was performed with a ZEISS EVO 50 EP. Raman spectroscopy was conducted with a LABRAM HR 800 UV HORIBA JOBIN YVON, using as a light source a laser with a wavelength of 785 nm. The Mo-foil/CZTS/CdS/Pt photoelectrode was fabricated through the CdS chemical bath deposition at 75 °C using a solution comprising thiourea, cadmium acetate, and ammonium hydroxide [21]. The platinum catalyst was photoelectrodeposited at −0.1 V vs. Ag/AgCl for 10 min in a 0.1 M Na_2SO_4 solution containing 1 mM of H_2PtCl_6. Photoelectrochemical characterization was performed in 0.5 M Na_2SO_4 buffered (phosphate-based) at pH = 6.5 under AM 1.5G solar irradiation at 100 mW cm^{-2} (1 sun) using Sunlite solar simulator by Abet Technologies.

Results and discussion

Bath formulation

The electrolytic bath (pH = 10) exploited both chloride and sulfate metallic precursors salts and potassium pyrophosphate ($K_4P_2O_7$) as the primary complexing agent [16, 17]. The complexation of the metallic ions, particularly Sn^{2+} [22], was indeed fundamental for the formulation of a stable solution because of the tendency to form precipitates. A similar observation was made for copper species whose pyrophosphate complex was already reported in the literature [23]. The addition of both tin and copper species causes a white precipitate formation due to the oxidation of non-complexed tin cations Sn(II) → Sn(IV). To contrast said phenomenon, the electrolyte's formulation sequence was defined as the dissolution of potassium pyrophosphate $K_4P_2O_7$, then $SnCl_2$, afterward $CuCl_2$, and finally $ZnSO_4$. Although the solution obtained was stable, precipitates formed after multiple depositions or voltammetric tests, probably due to local pH variations or the oxidation reactions occurring at the anode. This behavior may also be attributed to potassium pyrophosphate's inability to complex effectively Cu^{2+} cations, thus favoring the uncontrolled formation of metallic hydroxides/oxides. With this regard, the addition of EDTA-Na_2 after tin precursor salts, which is

known to be a strong copper sequestrant [24], proved to be effective in improving the chemical stability of the electrolyte [25, 26]. In fact, the formation of strongly complexed species avoided the tin species' oxidation with consequent precipitation of oxide powders.

Electrochemical characterization

The electrochemical behavior of the single metallic species was investigated through cyclic voltammetry (CV) at increasing EDTA-Na_2 concentration (1–15 mM) (Fig. 1). The pH was kept at 10 for the three electrolytes, replicating the same experimental condition of the co-electrodeposition bath (Fig. 2). The progressive addition of EDTA-Na_2 resulted in a more defined copper reduction peak, centered at −1 V vs. Ag/AgCl (Fig. 1a). Moreover, the smaller gap between reduction and oxidation peak indicated a higher degree of reversibility of the reaction when compared to the bare pyrophosphate bath. An opposite trend was found for the tin reduction peak that was progressively shifted towards more negative potential, going from −1.1 V vs. Ag/AgCl for the EDTA-free bath to −1.25 V vs. Ag/AgCl at the maximum concentration, while the oxidation peak was not affected (Fig. 1b). No

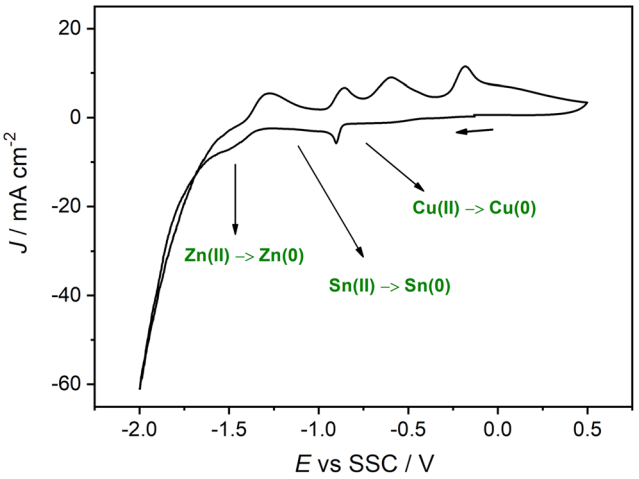

Fig. 2 Cyclic voltammetry in 230 mM of $K_4P_2O_7$, 15 mM of $CuCl_2$, 35 mM of $ZnSO_4$, 15 mM of EDTA-Na_2, 10 mM of $SnCl_2$, pH = 10 corrected with NH_4OH. [T = 25 °C, 20 mV s^{-1}]

significant changes were observed in the CV curve of the zinc solution, where the addition of the complexing agent resulted in smaller cathodic currents, corresponding to a lower amount of secondary reactions occurring at the working electrode surface. Zinc reduction peak was found at −1.5 V vs. Ag/AgCl, in the

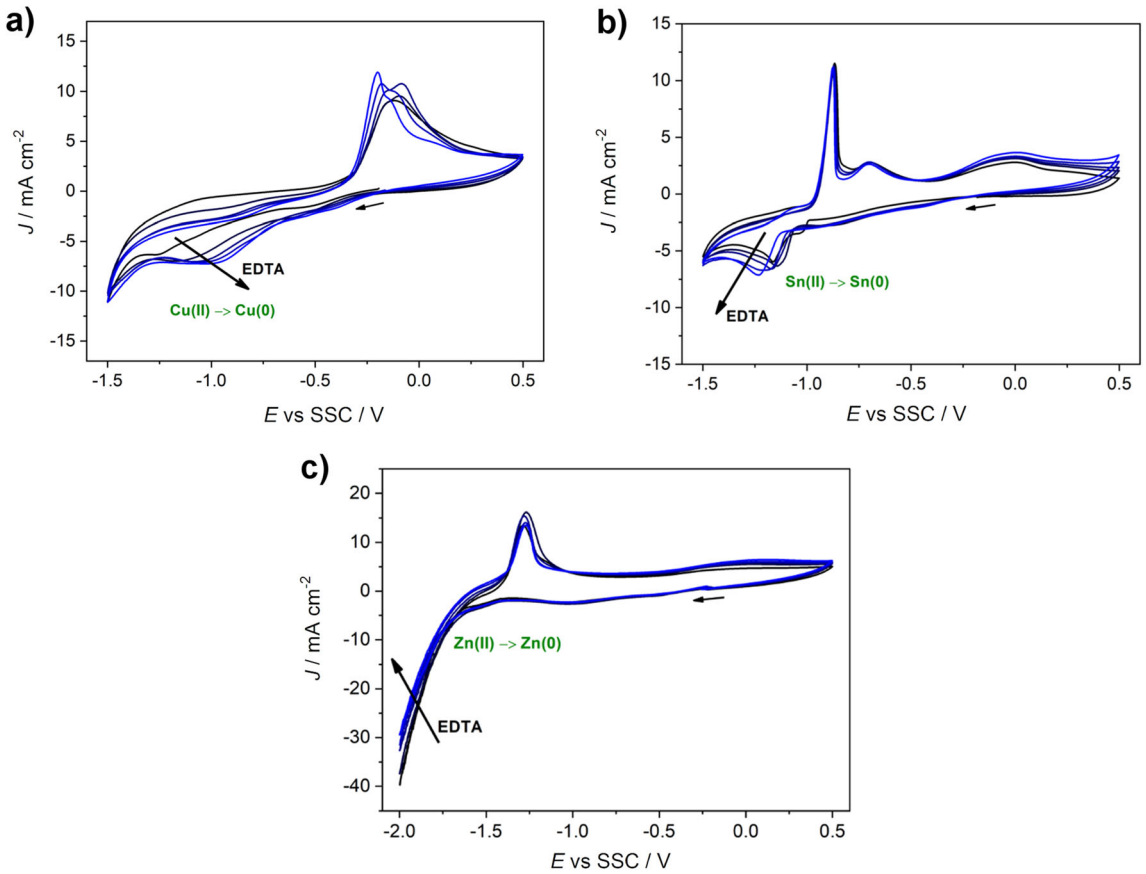

Fig. 1 Cyclic voltammetries of the single metal salt solution. ***a*** 230 mM of $K_4P_2O_7$, 15 mM of $CuCl_2$, 0–15 mM EDTA-Na_2. ***b*** 230 mM of $K_4P_2O_7$, 35 mM of $ZnSO_4$, 0–15 mM EDTA-Na_2. ***c*** 230 mM of $K_4P_2O_7$, 10 mM of $SnCl_2$, 0–15 mM EDTA-Na_2. [T = 25 °C, 20 mV s^{-1}, addition of 5 mM EDTA-Na_2 per step]

proximity of hydrogen evolution reaction (Fig. 1c). The addition of EDTA-Na_2 improved the electrolyte's electrochemical stability; thus, the highest concentration was selected (15 mM) for the co-electrodeposition bath. It is worth noticing that the addition of EDTA-Na_2 increased the acidity; hence, a higher amount of NH_4OH was required to reach pH = 10. Higher content of ammonium hydroxide helped stabilize further and increase the bath's shelf-life [27]. The CV curve of the co-electrodeposition bath showed three different peaks in agreement with the curves of the single metallic elements, indicating that the formulation was suitable for the deposition of Cu-Zn-Sn films (Fig. 2).

CZT electrodeposition and annealing

The CZT electrodeposition parameters were empirically determined through galvanostatic depositions, aiming at a film composition capable of limiting secondary phases after reactive annealing. Congruently, the target values of metals in the precursor were Cu 43.5 at. %, Zn 30 at. %, and Sn 26.5 at. %, commonly known as the Cu-poor Zn-rich precursor. Overall, the zinc deposited showed a linear correlation with the cathodic current density, while the concentration in the bath mainly determined the copper and tin composition. Because of the significant difference in the reduction potentials between the zinc ions and the copper and tin ones, the latter are expected to be deposited under mass transport limitation during the CZT film deposition. Therefore, the CZT precursor composition optimization was achieved by selecting an opportune Cu/Sn molar ratio in the electrolyte. The selected conditions for the co-electrodeposition process were −2.3 mA cm^{-2} for 10 min at 25 °C; the electrode potential increases during deposition reaching about −1.3 V vs Ag/AgCl. The electrodeposited layer showed a composition of Cu 44 ± 2 at. %, Zn 28 ± 1 at. %, and Sn 28 ± 2 at. % with an average thickness of 500 nm, measured by both XRF and EDX. The CZT samples showed a homogenous macroscopic appearance. SEM micrograph confirmed the homogeneity of the as-deposited precursor, showing a globular morphology (Fig. 3a). The CZT layer was soft annealed in a nitrogen atmosphere to improve the film crystallinity and promote intermetallic species formation, i.e., Cu_xZn_y and Cu_xSn_y, with beneficial effects on the quality of CZTS kesterite phase achieved upon reactive annealing in the sulfur atmosphere [28]. The thermal treatment lasted 90 min at 300 °C in an inert N_2 atmosphere at 1 bar, and a 20 °C min^{-1} ramping rate was selected [29, 30]. As expected, the annealing step resulted in the formation of $CuZn_5$ (JCPDS 35-1151) and

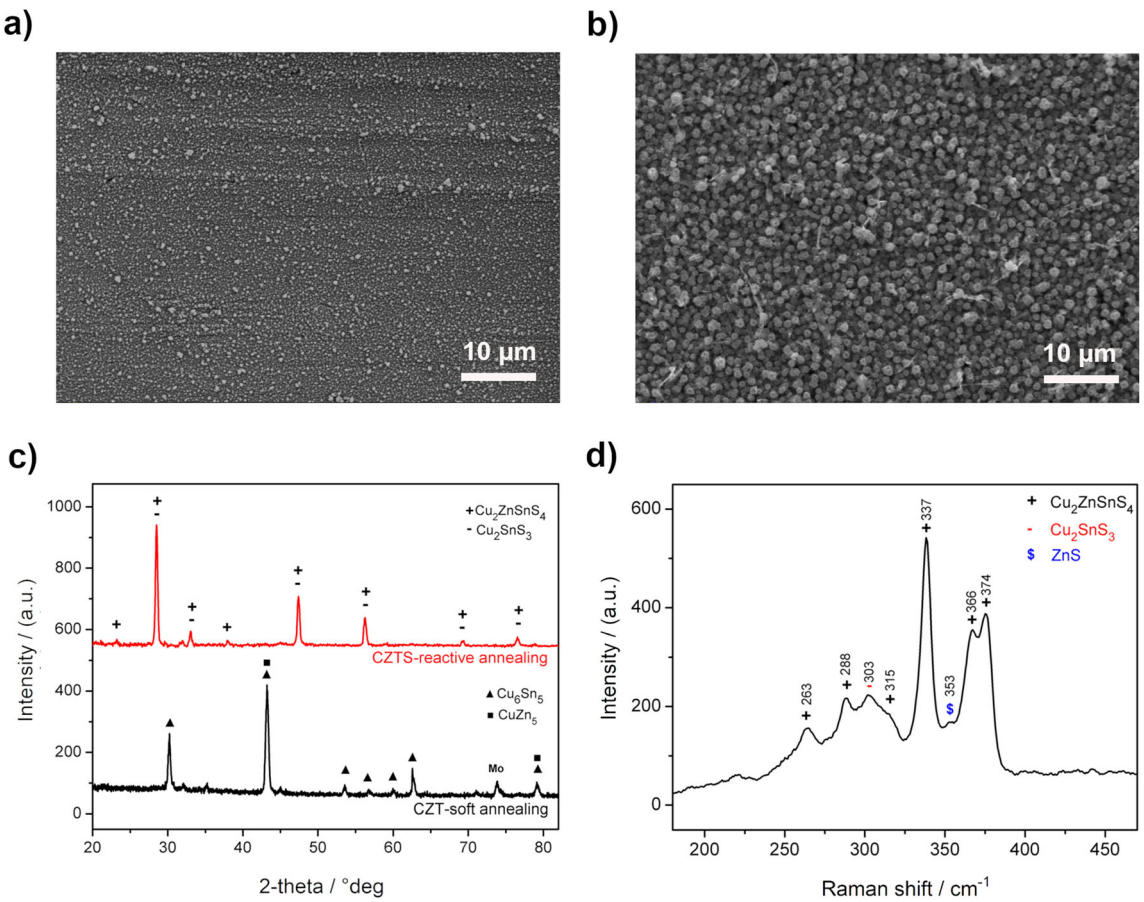

Fig. 3 SEM micrographs of **a** CZT precursor and **b** CZTS films. [scale bar: 10 µm] **c** XRD spectra of the CZT metallic precursor after soft annealing and CZTS after reactive annealing. **d** Raman spectrum of CZTS (785 nm laser source)

Cu_6Sn_5 (JCPDS 45-1488) phases while no peaks belonging to the single metallic elements were observed (Fig. 3c). The annealed samples were then sulfurized at 560 °C with 25 mg of sulfur in a tubular furnace for 30 min (20 °C min^{-1}, 1 bar N_2), followed by cooling outside the furnace. The SEM micrographs in Fig. 3a–b show the morphology of the as-deposited films and after sulfurization, respectively. As expected, the reactive annealing changed the film morphology, leading to larger grains. XRD diffractogram confirmed the predicted high-degree conversion from CZT to CZTS in the correct kesterite crystalline structure (JCPDS 26-0575). Figure 3c shows the XRD of the sulfurized films with the dominant reflection peaks at (112), (200), (220), (224), and (312) planes (Fig. 3c). The selection of a two-step thermal treatment was justified by the benefits of this approach: the avoidance of the formation of unwanted secondary phases, mainly copper-tin, zinc, and tin sulfides [31], whose presence is related to a reduced photoactivity of the film [32]. Complementary Raman spectroscopy confirmed the presence of the CZTS phase, together with minor sulfide phases. Figure 3d shows the typical Raman peaks of CZTS at 263 cm^{-1}, 288 cm^{-1}, 337 cm^{-1}, 366 cm^{-1}, and 374 cm^{-1} which is commonly observed in literature when the 785-nm excitation wavelength of the laser source is used [30]. Minor Raman peaks corresponding to cubic-Cu_2SnS_3 and ZnS were also observed at 303 cm^{-1} and 353 cm^{-1} respectively. The fractured surface of the CZTS film (Fig. 4) agreed with the XRD and Raman data; no visible secondary phases were observed through SEM imaging. The film was characterized by a compact layer in the proximity of the molybdenum substrate while the surface showed different clusters, as shown by the top surface micrograph (Fig. 3b). The formation of the kesterite phase resulted in a volumetric expansion of about 2.3 times, considering a precursor thickness of ~500 nm, which resulted in a CZTS film thickness of about 1.2 μm (Fig. 4).

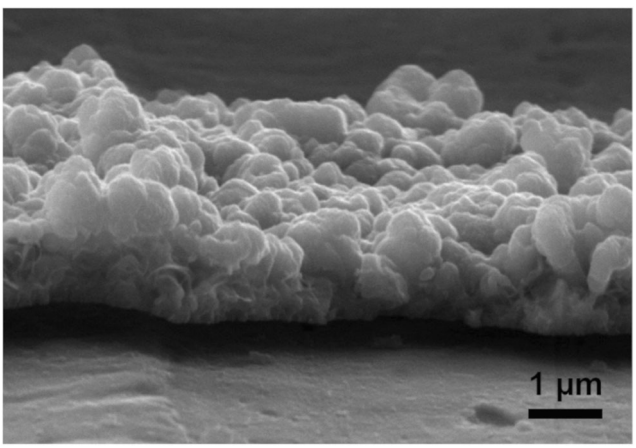

Fig. 4 SEM micrograph of the cross-section of the CZTS film on flexible molybdenum substrate

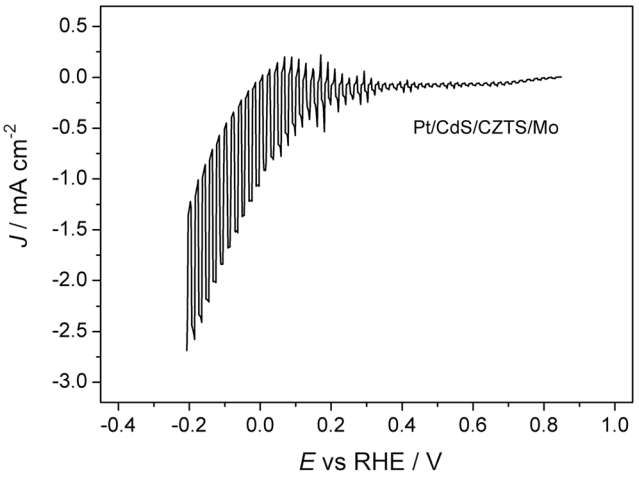

Fig. 5 Photoelectrochemical characterization of the flexible CZTS-based photoelectrode in 0.5 M Na_2SO_4 solution buffered at pH 6.5, under intermittent (0.5 Hz) AM 1.5G solar irradiation at 100 mW/cm^2

Photoelectrochemical test

The photoactivity of the kesterite film (p-type) was investigated through a photoelectrochemical test, evaluating the ability of the material to trigger water electrolysis at increasing cathodic bias under 1 sun condition. The characterization was carried out in a 0.5 M Na_2SO_4 solution, buffered at pH = 6.85, using a solar simulator with an intermittent (0.5 Hz) light source (Fig. 5). The test consisted of linear sweep voltammetry, carried out under chopped illumination. The surface potential values were reported to the reversible hydrogen electrode (RHE) $E_{RHE}=E+E_{SSC}$ +(0.059 pH). The photoelectrode fabrication also comprised the deposition of CdS (n-type) thin-film onto CZTS, followed by Pt nanoparticles photo-electrodeposition: the former acted as a buffer layer to improve photo-charges separation. At the same time, the latter increased the electron transfer to the electrolyte. Upon illumination, a progressive increase of the reduction current at more cathodic biases was observed, indicating the p-type character of the synthesized film (Fig. 5). The photo-assisted water splitting performance was evaluated at 0 V vs. RHE, the thermodynamic potential value of the hydrogen evolution reaction (HER), resulting in a photocurrent of 1.01 mA cm^{-2}. This value is coherent with the results reported for CZTS/CdS/Pt photoelectrodes on SLG/Mo substrate [33–38], in the order of a few mA cm^{-2}, demonstrating the viability of the investigated synthesis method on flexible substrates.

Conclusions

The use and effectiveness of an alkaline plating bath for CZT co-electrodeposition have been demonstrated. The addition of the two complexing agents $K_4P_2O_7$ and EDTA-Na_2 showed a beneficial effect on the stability and replicability of the

precursor's composition, with variations only up to 2% at. After sulfurization, the target kesterite phase was obtained, preventing the formation of any MoS_2 and minimizing the presence of undesired phases. Photoelectrochemical characterization showed a significant photoactivity (1.01 mA cm^{-2} of photocurrent), demonstrating the p-type character of the absorber film.

Funding Open access funding provided by Politecnico di Milano within the CRUI-CARE Agreement

References

1. Green MA, Dunlop ED, Levi DH, Hohl-Ebinger J, Yoshita M, Ho-Baillie AWY (2019) Solar cell efficiency tables (version 54). Prog Photovolt Res Appl 27(7):565–575. https://doi.org/10.1002/pip.3171
2. Ito K, Nakazawa T (1988) Electrical and optical properties of stannite-type quaternary semiconductor thin films. Jpn J Appl Phys 27:2094–2097. https://doi.org/10.1143/JJAP.27.2094 Part 1, No. 11
3. Colombara D, Crossay A, Vauche L, Jaime S, Arasimowicz M, Grand PP, Dale PJ (2015) Electrodeposition of kesterite thin films for photovoltaic applications: Quo vadis? Phys Status Solidi 212(1):88–102. https://doi.org/10.1002/pssa.201431364
4. Manivannan R, Victoria SN (2018) Preparation of chalcogenide thin films using electrodeposition method for solar cell applications – A review. Sol Energy 173:1144–1157
5. Unveroglu B, Zangari G (2016) Towards phase pure kesterite CZTS films via Cu-Zn-Sn electrodeposition followed by sulfurization. Electrochim Acta 219:664–672. https://doi.org/10.1016/j.electacta.2016.10.079
6. Scragg JJ, Dale PJ, Peter LM, Zoppi G, Forbes I (2008) New routes to sustainable photovoltaics: Evaluation of Cu 2ZnSnS4 as an alternative absorber material. Phys Status Solidi Basic Res 245(9):1772–1778. https://doi.org/10.1002/pssb.200879539
7. Zhang Y, Ye Q, Liu J, Chen H, He X, Liao C, Han J, Wang H, Mei J, Lau WM (2014) Earth-abundant and low-cost CZTS solar cell on flexible molybdenum foil. RSC Adv 4(45):23666–23669. https://doi.org/10.1039/c4ra02064b
8. Agasti A, Mallick S, Bhargava P (2018) Electrolyte pH dependent controlled growth of co-electrodeposited CZT films for application in CZTS based thin film solar cells. J Mater Sci Mater Electron 29(5):4065–4074. https://doi.org/10.1007/s10854-017-8350-z
9. Gur E, Saritas S, Demir E, et al (2019) CZTS growth for solar cell application by electrochemical deposition: pH effect. In: Proceedings of the 2019 IEEE Regional Symposium on Micro and Nanoelectronics, RSM 2019. Institute of Electrical and Electronics Engineers Inc. 123–125
10. Hreid T, O'Mullane AP, Spratt HJ, Will G, Wang H (2016) Investigation of the electrochemical growth of a Cu–Zn–Sn film on a molybdenum substrate using a citrate solution. J Appl Electrochem 46(7):769–778. https://doi.org/10.1007/s10800-016-0967-8
11. Toura H, Khattak YH, Baig F, Soucase BM, Touhami ME, Hartiti B (2019) Effect of complexing agent on the morphology and annealing temperature of CZTS kesterite thin films by electrochemical deposition. Curr Appl Phys 19(5):606–613. https://doi.org/10.1016/j.cap.2019.03.003
12. Sani R, Manivannan R, Noyel Victoria S (2018) One step electrodeposition of copper zinc tin sulfide using sodium thiocyanate as complexing agent. J Electrochem Sci Technol 9(4):308–319. https://doi.org/10.5229/JECST.2018.9.4.308
13. Paraye A, Sani R, Ramachandran M, Selvam NV (2018) Effect of pH and sulfur precursor concentration on electrochemically deposited CZTS thin films using glycine as the complexing agent. Appl Surf Sci 435:1249–1256. https://doi.org/10.1016/j.apsusc.2017.11.210
14. Azmi S, Nohair M, El Marrakchi M, et al (2018) Effect of the complexing agents on the properties of electrodeposited CZTS thin films. In: 7th International IEEE Conference on Renewable Energy Research and Applications, ICRERA 2018. Institute of Electrical and Electronics Engineers Inc. 1346–1351
15. Beres M, Syzdek J, Yu KM, Mao SS (2018) Growth behavior of co-electrodeposited CZTS precursor thin films from acidic baths containing tartaric acid. Mater Chem Phys 204:83–94. https://doi.org/10.1016/j.matchemphys.2017.09.071
16. Clauwaert K, Binnemans K, Matthijs E, Fransaer J (2016) Electrochemical studies of the electrodeposition of copper-zinc-tin alloys from pyrophosphate electrolytes followed by selenization for CZTSe photovoltaic cells. Electrochim Acta 188:344–355. https://doi.org/10.1016/J.ELECTACTA.2015.12.013
17. Brenner A (2013) Electrodeposition of alloys: principles and practice. Elsevier
18. Khalil MI, Bernasconi R, Pedrazzetti L, Lucotti A, Donne AL, Binetti S, Magagnin L (2017) Co-electrodeposition of metallic precursors for the fabrication of CZTSe thin films solar cells on flexible Mo foil. J Electrochem Soc 164(6):D302–D306. https://doi.org/10.1149/2.1001706jes
19. Khalil MI, Bernasconi R, Ieffa S, Lucotti A, le Donne A, Binetti S, Magagnin L (2015) Effect of co-electrodeposited Cu-Zn-Sn precursor compositions on sulfurized CZTS thin films for solar cell. ECS Trans 64(29):33–41. https://doi.org/10.1149/06429.0033ecst
20. Khalil MI, Bernasconi R, Lucotti A, le Donne A, Mereu RA, Binetti S, Hart JL, Taheri ML, Nobili L, Magagnin L (2020) CZTS thin film solar cells on flexible Molybdenum foil by electrodeposition-annealing route. J Appl Electrochem 51(2):209–218. https://doi.org/10.1007/s10800-020-01494-1
21. Le Donne A, Marchionna S, Garattini P et al (2015) Effects of CdS buffer layers on photoluminescence properties of Cu2ZnSnS4 solar cells. Int J Photoenergy 2015:1–8. https://doi.org/10.1155/2015/583058
22. Duffield JR, Williams DR, Kron I (1991) Speciation studies of the solubility and aqueous solution chemistry of tin(II)- and tin(IV)-pyrophosphate complexes
23. Heitner-Wirguin C, Kendy J (1961) An ion exchange study of copper pyrophosphate complexes in solution. J Inorg Nucl Chem 22(3-4):253–257. https://doi.org/10.1016/0022-1902(61)80441-7
24. Khalil AH, Alquzweeni SS, Modhloom HM (2015) Removal of copper ions from contaminated soil by enhanced soil washing. Int J Environ Res 9:1141–1146. https://doi.org/10.22059/ijer.2015.1003

25. Gyliene O, Aikaite J, Nivinskiene O (2004) Recovery of EDTA from complex solution using Cu(II) as precipitant and Cu(II) subsequent removal by electrolysis. J Hazard Mater 116(1-2):119–124. https://doi.org/10.1016/j.jhazmat.2004.08.026
26. Mkawi EM, Ibrahim K, Ali MKM, Farrukh MA, Mohamed AS, Allam NK (2014) Effect of complexing agents on the electrodeposition of Cu–Zn–Sn metal precursors and corresponding Cu2ZnSnS4-based solar cells. J Electroanal Chem 735:129–135. https://doi.org/10.1016/J.JELECHEM.2014.10.021
27. Hathaway BJ, Tomlinson AAG (1970) Copper(II) ammonia complexes. Coord Chem Rev 5(1):1–43. https://doi.org/10.1016/S0010-8545(00)80073-9
28. Ahmed S, Reuter KB, Gunawan O, Guo L, Romankiw LT, Deligianni H (2012) A high efficiency electrodeposited Cu 2ZnSnS 4 solar cell. Adv Energy Mater 2:253–259. https://doi.org/10.1002/aenm.201100526
29. Jiang F, Ikeda S, Harada T, Matsumura M (2014) Pure Sulfide Cu2ZnSnS4 thin film solar cells fabricated by preheating an electrodeposited metallic stack. Adv Energy Mater 4(7):1301381. https://doi.org/10.1002/aenm.201301381
30. Fernandes PA, Salomé PMP, da Cunha AF (2011) Study of polycrystalline Cu2ZnSnS4 films by Raman scattering. J Alloys Compd 509(28):7600–7606. https://doi.org/10.1016/J.JALLCOM.2011.04.097
31. Gurav KV, Pawar SM, Shin SW, suryawanshi MP, Agawane GL, Patil PS, Moon JH, Yun JH, Kim JH (2013) Electrosynthesis of CZTS films by sulfurization of CZT precursor: effect of soft annealing treatment. Appl Surf Sci 283:74–80. https://doi.org/10.1016/j.apsusc.2013.06.024
32. Kumar M, Dubey A, Adhikari N, Venkatesan S, Qiao Q (2015) Strategic review of secondary phases, defects and defect-complexes in kesterite CZTS-Se solar cells. Energy Environ Sci 8(11):3134–3159. https://doi.org/10.1039/c5ee02153g
33. Yokoyama D, Minegishi T, Jimbo K, et al (2010) H2 evolution from water on modified Cu2ZnSnS 4 photoelectrode under solar light. Appl Phys Express 3 https://doi.org/10.1143/APEX.3.101202
34. Ma G, Minegishi T, Yokoyama D, Kubota J, Domen K (2011) Photoelectrochemical hydrogen production on Cu2ZnSnS 4/Mo-mesh thin-film electrodes prepared by electroplating. Chem Phys Lett 501(4-6):619–622. https://doi.org/10.1016/j.cplett.2010.11.081
35. Wang P, Minegishi T, Ma G, Takanabe K, Satou Y, Maekawa S, Kobori Y, Kubota J, Domen K (2012) Photoelectrochemical conversion of toluene to methylcyclohexane as an organic hydride by Cu 2ZnSnS 4-based photoelectrode assemblies. J Am Chem Soc 134(5):2469–2472. https://doi.org/10.1021/ja209869k
36. Rovelli L, Tilley SD, Sivula K (2013) Optimization and stabilization of electrodeposited Cu2ZnSnS 4 photocathodes for solar water reduction. ACS Appl Mater Interfaces 5(16):8018–8024. https://doi.org/10.1021/am402096r
37. Jiang F, Gunawan HT et al (2015) Pt/In2S3/CdS/Cu2ZnSnS4 thin film as an efficient and stable photocathode for water reduction under sunlight radiation. J Am Chem Soc 137(42):13691–13697. https://doi.org/10.1021/jacs.5b09015
38. Tay YF, Kaneko H, Chiam SY, Lie S, Zheng Q, Wu B, Hadke SS, Su Z, Bassi PS, Bishop D, Sum TC, Minegishi T, Barber J, Domen K, Wong LH (2018) Solution-processed Cd-substituted CZTS photocathode for efficient solar hydrogen evolution from neutral water. Joule 2(3):537–548. https://doi.org/10.1016/j.joule.2018.01.012